Science of the Total Environment 824 (2022) 153818

Contents lists available at ScienceDirect

Science of the Total Environment

journal homepage: www.elsevier.com/locate/scitotenv

Potential toxicity of inorganic ions in particulate matter: Ion permeation in lung and disruption of cell metabolism

Sujin Park [a,b,1], Jayoung Ku [a,c,1], Sung-Min Lee [d], Huiseon Hwang [d], Namseok Lee [a,c], Hanul Kim [a,b], Ki-Jun Yoon [d], Yoosik Kim [a,c,*], Siyoung Q. Choi [a,b,*]

[a] Department of Chemical and Biomolecular Engineering, Korea Advanced Institute of Science and Technology (KAIST), Daejeon 34141, South Korea
[b] KAIST Institute for the NanoCentury, Korea Advanced Institute of Science and Technology (KAIST), Daejeon 34141, South Korea
[c] KAIST Institute for Health Science and Technology (KIHST), Korea Advanced Institute of Science and Technology (KAIST), Daejeon 34141, South Korea
[d] Department of Biological Sciences, Korea Advanced Institute of Science and Technology (KAIST), Daejeon 34141, South Korea

HIGHLIGHTS

- Biological effects of inorganic ions in particulate matter were investigated.
- Water-soluble inorganic ions rapidly penetrate the surfactant layer in the lungs.
- Nitrate and sulfate ions are responsible for perturbing gene expression in the lungs.
- Exposure to inorganics activates cell metabolism such as tumorigenesis and immunity.
- Inorganic ion mixture leads to a unique synergistic gene expression pattern.

GRAPHICAL ABSTRACT

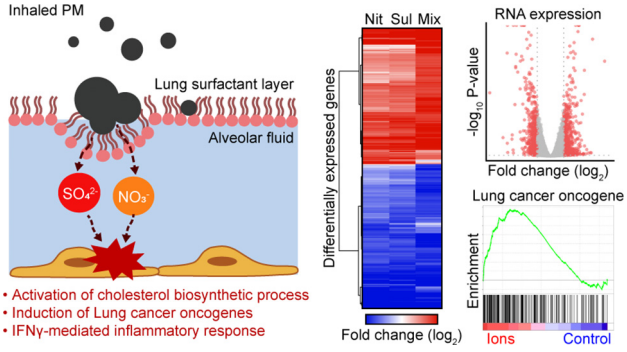

ARTICLE INFO

Article history:
Received 11 November 2021
Received in revised form 8 February 2022
Accepted 8 February 2022
Available online 11 February 2022

Editor: Lotfi Aleya

Keywords:
PM
Lung surfactant
Water-soluble ions
High-throughput RNA sequencing
Cellular metabolism
Tumorigenesis

ABSTRACT

Exposure to ambient particulate matter (PM) is associated with adverse health effects. Yet, due to the complexity of its chemical composition, the molecular effects of PM exposure and the mechanism of PM-mediated toxicity remain largely unknown. Here, we show that water-soluble inorganics such as nitrate and sulfate ions, rather than PM itself, rapidly penetrate the lung surfactant barrier to the alveolar region and perturb gene expression in the lungs. Through high-throughput sequencing of lung adenocarcinoma cells, we find that exposure to nitrate and sulfate ions activates the cholesterol biosynthetic metabolism and induces the expression of genes related to tumorigenesis. Transcriptome analysis of mouse lungs exposed to nitrate/sulfate aerosols reveals interferon gamma-associated immune response. Interestingly, we find that exposure to a nitrate/sulfate mixture leads to a unique gene expression pattern that is not observed when nitrate or sulfate is treated alone. Our work suggests that the water-soluble ions are a potential source of PM-mediated toxicity and provides a roadmap to unveil the molecular mechanism of health hazards from PM exposure.

Abbreviations: PM, particulate matter; GO, gene ontology; GSEA, gene set enrichment analysis; IFNγ, interferon gamma; DLS, dynamic light scattering; IC, ion chromatography; DPPC, 1,2-dipalmitoyl-sn-glycero-3-phosphocholine; DPPG, 1,2-dipalmitoyl-sn-glycero-3-phospho-rac-(1-glycerol); FBS, fetal bovine serum; ATCC, American type culture collection; RT-qPCR, reverse transcription-quantitative PCR; MSigDB, molecular signatures database; WT, wild-type; SPF, specific pathogen-free; IACUC, institutional animal care and use committee; SMPS, scanning mobility particle sizer; CPC, condensation particle counter; PFA, paraformaldehyde; NGS, next generation sequencing; WGS, whole genome sequencing; SNV, single nucleotide variant; IC50, 50% inhibitor concentration; DEG, differentially expressed gene; SS, semantic similarity; NES, normalized enrichment score; NKT, natural killer T; IFNα, interferon alpha; IFNβ, interferon beta.

* Corresponding authors at: Department of Chemical and Biomolecular Engineering, Korea Advanced Institute of Science and Technology (KAIST), Daejeon 34141, South Korea.
E-mail addresses: ysyoosik@kaist.ac.kr (Y. Kim), sqchoi@kaist.ac.kr (S.Q. Choi).

[1] Both authors contributed equally to this work.

http://dx.doi.org/10.1016/j.scitotenv.2022.153818

1. Introduction

With increasing concerns about human exposure to ambient particulate matter (PM), the potential effect of inhaled PM on human health, including respiratory diseases and cardiovascular diseases, is a growing issue (Hoek et al., 2013; Kim et al., 2015; Valavanidis et al., 2008; World Health Organization, 2016). The cellular and molecular effects of PM particles have been evaluated to understand the relationship between PM toxicity and human diseases. For example, a wide range of cellular effects of PM-mimic particles has been reported such as oxidative stress, genotoxicity, inflammatory response, and lipid droplet formation (Bourdon et al., 2012; Cao et al., 2015; Davoren et al., 2007; Hemmingsen et al., 2011; Park et al., 2018). However, such broad and seemingly uncorrelated cellular responses make it difficult to pinpoint their molecular effects. One possibility is the complexity of PM composition. Because the PM composition utterly varies based on its source and formation process, it is difficult to create a clear link between the chemical constituents of PM and their biological effects. There have been a few attempts to identify the responsible components and their biological impacts, such as respiratory disease, cardiovascular disease, and lung cancer (Lippmann et al., 2013; Wyzga and Rohr, 2015). However, these attempts were limited to explaining the association between PM composition and health outcomes after short- and long-term exposure to PM, and consequently, our understanding of the molecular effects of the specific components is limited.

In addition to the chemical diversity and complexity of PM, the methods of applying the particles could be a reason for their broad cellular effects. Because the particles have been applied directly to an experimental target by particle dispersion or as a supplement in cell culture medium, it is likely that the cellular responses observed in the previous *in vitro* studies were primarily driven by the direct particle-cell interactions, particularly particle internalization. However, in real situations, such direct interaction is unlikely to occur. Particles inhaled into the deep lung must interact with a lipid-rich lung surfactant layer covering the alveolar surface (Veldhuizen and Haagsman, 2000; Veldhuizen et al., 1998; Wang et al., 2020) before they can contact the alveolar cells (Fig. 1). Because this thin surfactant film serves as a protecting barrier against inhaled pathogens and aerosols (Han and Mallampalli, 2015), the PM-surfactant layer interaction must be considered. Previously, it was found that PM particles inhibit the biophysical function of lung surfactants by hindering molecular packaging and forming surfactant-particle aggregates (Arick et al., 2015; Beck-Broichsitter et al., 2011; Dwivedi et al., 2014; Harishchandra et al., 2010). For the particles passing through the surfactant layer, the adsorption of surfactants to particles can diminish the contact of particles with cellular membranes and can inhibit further particle-cell interactions (Radiom et al., 2020; Vranic et al., 2013). This inhibition may also significantly alter the toxicological effects of the inhaled particles.

Considering the protective role of the lung surfactant layer that inhibits the direct particle-cell interactions, the permeability of each PM component through the surfactant layer must be considered in advance. Hence, we focus on the effect of the water-soluble ionic components, which comprise a large portion of PM, from 10 to 50% of the total PM2.5 mass (Karthikeyan and Balasubramanian, 2006; Shon et al., 2012; Son et al., 2012), on cells after the particle adsorption to the surfactant layer. Because these inorganics are soluble in water, they can easily dissolve in the wet alveolar walls during pulmonary retention of the inhaled particle. Previous studies used the atmospheric concentrations of ionic components in PM to understand how they might trigger respiratory diseases (Cao et al., 2012; Hwang et al., 2017; Maynard et al., 2007). However, applying atmospheric

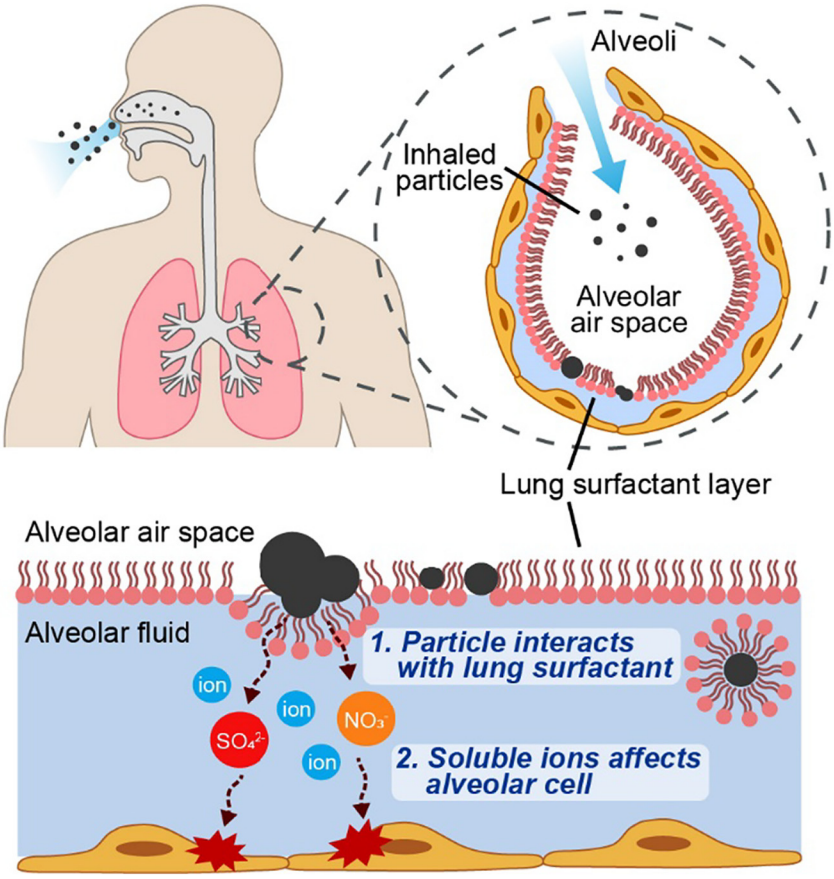

Fig. 1. Schematic illustrations of airborne particle inhalation into alveoli. Inhaled particles must interact with the lung surfactant layer at the air/water interface of the alveoli. Direct interaction between the inhaled particle and the alveolar cell is inhibited by the surfactant, whereas water-soluble ionic components can easily dissolve in the wet alveolar wall and affect the alveolar cells.

concentration is questionable as the penetration efficiency of these PM inorganic ions through the surfactant layer is unknown. In addition, the molecular effects induced by the exposure to inorganic ions of PM remain uninvestigated.

In this study, we attempt to answer how much inorganic ions in PM particles can penetrate through the surfactant layer of the lungs following the adsorption of particles and how the penetrated ions perturb the gene expression of lung epithelial cells (Fig. S1). The lipid monolayer composed of 1,2-Dipalmitoyl-sn-glycero-3-phosphocholine (DPPC) and 1,2-Dipalmitoyl-sn-glycero-3-phospho-rac-(1-glycerol) (DPPG) in the molar ratio of 4:1 was adopted as a model lung surfactant layer. The monolayer of this composition has been widely adopted to mimic the pulmonary surfactant monolayer (Hu et al., 2020; Saad et al., 2009). Ion permeation through the surfactant layer was analyzed using two commercially available standard reference PMs, representing PMs from different sources, collected from a diesel vehicle and a road tunnel, respectively. The genome-wide gene expression changes induced by the exposure to nitrate and/or sulfate ions, the two major components of PM, were investigated through RNA sequencing of human lung adenocarcinoma cells and mouse lung tissues. Collectively, our study provides a comprehensive genome-wide analysis to provide the molecular effects of ambient PM exposure and suggests that the water-soluble inorganic ions of PM may act as a major source of PM-mediated health hazards.

2. Materials and methods

2.1. Characteristics of particulate matter

Diesel Particulate Matter NIST-2975 (Diesel PM, NIST® SRM® 2975) and PM10-like Fine Dust ERM-CZ100 (Fine Dust, ERM® certified reference material) were purchased from Sigma-Aldrich (St. Louis, MO). The hydrodynamic size distributions of each particle in deionized water and buffer were measured with dynamic light scattering (DLS) (Zetasizer Nano ZS, Malvern Instruments). The mass concentration of the five major ionic species, Na^+, NH_4^+, Cl^-, NO_3^- and SO_4^{2-}, was analyzed by ion chromatography (IC) (883 Basic IC Plus, Metrohm). For the IC measurement, a 5 mg/mL dispersion solution in water was sonicated for 3 h at 25 °C for complete extraction of the water-soluble components and filtered through a 0.2 μm syringe filter (Whatman) before the analysis. The calibration graph was obtained by injecting a known concentration of each ion in the range of 1–20 ppm, and the concentrations of ions in the samples were calculated directly from the calibration curve.

2.2. Formation of phospholipid monolayer and Langmuir isotherm

DPPC and DPPG (4:1 mol%) were dissolved in chloroform to a 1 mM concentration. The lipid/Diesel PM mixture was prepared by mixing particles with lipid solution in a 1:1 weight ratio. The lipid solution or lipid/particle solution was gently spread out drop by drop on the air/water interface in the customized Langmuir trough (250 mm × 140 mm × 16 mm), filled with the aqueous buffer (100 mM NaCl and 10 mM HEPES, pH 7.4). After 30 min for the equilibration, the monolayer, compressed at a constant rate of 9 cm^2/min. The surface pressure at the air/water interface was measured using a Wilhelmy tensiometer (Riegler & Kirstein GmbH) and filter paper.

2.3. Dynamic light scattering

To characterize the submerged particles during compressions, an aqueous subphase under the lipid/Diesel PM layer was collected before and after three compression/expansion cycles. The hydrodynamic size distribution of the particles in the collected subphase was measured by DLS (Zetasizer Nano ZS, Malvern Instruments).

2.4. Langmuir-Schaefer film and scanning electron microscopy

To characterize the particles at the air/water interface, the molecular film at the air/water interface was transferred to a mica surface (highest grade mica disk 9.9 mm, Ted Pella Inc.) attached to a piece of slide glass and a glass supporting fixture (diameter = 20 mm, height = 15 mm) using the inverse Langmuir-Schaefer method. At a surface pressure of 30 mN/m, the water in the trough was removed through gentle aspiration until the vertical height of the air/water interface was lower than that of the mica surface. The mica was covered with paper to prevent settling of the desorbed particles during the compression, and the paper was gently removed right before the aspiration. After complete evaporation of the residual water on the mica surface, the particles transferred to the mica surface were visualized using scanning electron microscopy (SEM, S-4800, Hitachi). For clear visualization, a 10–50 nm-thick platinum film was deposited on the surface.

2.5. Ion chromatography

A petri dish (diameter = 50 mm) was filled with 5 mL deionized water, and then, a lipid monolayer was formed at the air/water interface by spreading the lipid solution with an initial surface pressure of 20 mN/m. After equilibration, 5 mg of Diesel PM or Fine Dust was gently spread on the lipid monolayer *via* powder spray or drop by drop spreading of a chloroform solution and left unperturbed at 24 °C with 88% humidity. After 24 h, the aqueous subphase was collected using a syringe pump (Legato 110, KDScientific). All solutions were filtered through a 0.2 μm syringe filter (Whatman) before the IC analysis. The mass concentration of the ionic species was calculated through normalization of the ion concentration from the IC results by the particle mass concentration of the analyzed solutions.

2.6. Human cell line and ammonium salt treatment

A549 lung adenocarcinoma cell line was cultured in RPMI media (Welgene) supplemented with 9.1% fetal bovine serum (FBS; Gibco) in a 37 °C and 5% CO_2 humidified incubator. The cell line was purchased from the American Type Culture Collection (ATCC) and authenticated through short tandem repeat (STR) genotyping. To treat the human cell line with an ammonium salt, the cells were grown in fresh media containing ammonium salt at the desired concentration for 2 days.

2.7. Cell viability test

The 3-(4,5-dimethylthiazol-2-yl)-2,5-diphenyl-2H-tetrazolium bromide (MTT) assay was performed to measure the cell viability after the ammonium salt treatment. 50,000 cells were seeded on a 6-well plate. After cell attachment, the media was changed to fresh media containing ammonium salt at the desired concentration. After 2 days, 20 μL of MTT solution (5 mg/mL in PBS, filtered; Invitrogen) was added, and the cells were incubated for 3.5 h at 37 °C in a humidified 5% CO_2 incubator. The supernatant was carefully removed and cells were resuspended in 100 μL of dimethylsulfoxide. The absorbance was measured at 545 nm using a Varioskan Lux microplate reader (ThermoFisher Scientific).

2.8. RNA extraction and reverse transcription-quantitative PCR (RT-qPCR)

To extract total RNA from the cells and mouse lungs, TRIsure (Bioline) and TRIzol (Invitrogen) were used, respectively. Following precipitation, DNase I (Takara) was treated, and purified RNA was reverse transcribed with RevertAid reverse transcriptase (Thermo Scientific) using random hexamers (Invitrogen). Synthesized cDNA was amplified by SensiFAST SYBR Lo-Rox Kit (Bioline) and analyzed using the AriaMx Real-Time PCR System (Agilent) or QuantStudio 1 (Applied Biosystems). Hierarchical clustering was performed using the complete method based on Euclidean distance values. The list of RT-qPCR primers is summarized in Supplementary Table 1.

2.9. RNA sequencing library preparation and data processing

2 × 101 paired-end mRNA sequencing libraries were constructed using the TruSeq Stranded mRNA LT Sample Prep Kit and sequenced by the NovaSeq 6000 (Illumina). Raw paired-end RNA sequencing reads were mapped to the reference human or mouse genome (build hg38 or mm10) with HISAT2 v2.1.0 (D. Kim et al., 2019) using default parameters except with the option "–rna-strandness RF." Only uniquely and concordantly mapped reads were then used for further analyses. To assign and summarize reads to genomic features, the feature Counts function of the Rsubread v2.4.2 (Liao et al., 2019) R package was used with transcriptome information from the GENCODE v27 or vM25. For the GENCODE, only reliable protein-coding transcripts that have a transcript_support_level of 1 or 2 were used. DESeq2 v1.30.1 (Love et al., 2014) R package analyzed the differentially expressed genes (DEGs) with the summarized raw read counts for each gene. For the RNA sequencing analysis of human cells, a shrinkage method with a type of 'apeglm' estimator (Zhu et al., 2019) was used to remove the noise and to preserve large differences. Following definitions for DEGs were applied: $|\log_2$ fold change$| > 1.5$ and P-value < 0.01 for the cells treated with the ammonium salt at a high concentration and $|\log_2$ fold change$| > 1$ and P-value < 0.01 for the others. Clustering biological functions using Gene Ontology and semantic similarity analysis was performed with the ViSEAGO v1.4.0 (Brionne et al., 2019) R package. Ensembl Release 104 was used as the GO database. For the GSEA of the cells treated with ammonium salts, genes were ranked based on the $\log_2$ fold change from the RNA sequencing analysis. Gene sets from the Molecular Signatures Database (MSigDB) v7.4 were loaded into the GSEA v4.1.0 (Mootha et al., 2003; Subramanian et al., 2005) software and analyzed. The accession number for the high throughput sequencing data reported in this study is GSE182629 (NCBI GEO DataSets).

2.10. Neutral lipid staining

To visualize the lipid metabolism in cells, HCS LipidTOX Green Neutral Lipid Stain and HCS LipidTOX Red Phospholipid Detection Reagent (Invitrogen) were used. Briefly, cells were plated onto 0.1% gelatin-coated glass-bottom confocal dish. The cells were fixed with 4% paraformaldehyde (PFA) (in PBS) for 10 min at RT and permeabilized with 0.1% Triton X-100 (in PBS) for 10 min at RT. Cells were then stained with the LipidTOX probes with a 1/1000 dilution ratio. DAPI (Invitrogen) was used to counterstain the nuclei. Cells were then mounted on a slide glass using SlowFade Diamond Antifade Mountant. Confocal microscopy was carried out using a ZEISS LSM 780 (Carl Zeiss) with a 63× objective.

2.11. Animals

All animal experiments were conducted with ICR wild-type (WT) mice obtained from DBL. To present a pregnant state, time pregnant female mice (TP11–TP18) were used. Before the experiments, all animals were housed under specific pathogen-free (SPF) conditions. The animal facility was regulated at 22 ± 2 °C and 50 ± 10% humidity with a 12 h interval of light and dark cycle and a constant temperature. During the experiment, each group of mice was raised under separated conditions in the exposed group and non-exposed group with food and water provided *ad libitum*. Food and water were limited during the exposure time. All animal procedures used in this study were performed following the protocol approved by the Institutional Animal Care and Use Committee (IACUC) of KAIST (IRB approval number: KA2021-097).

2.12. PM exposure design for the animal model

Female mice were separated into two groups (3–4 mice per group): exposed and non-exposed. Two groups were habited in different chambers in which both had an inlet and outlet of tubing. Only the inlet of a chamber for the exposed group was connected with air-tubing that was linked to a particulate generator (Model 3076, TSI, USA). The aerosol of the ammonium nitrate/sulfate mixture was generated with a particulate generator that compressed and dry air (CAS No. 132259-10-0) passed through an orifice to create an air jet breaking up the solution. This wet air including the aerosol passed through a dryer, which was filled with silica beads to be dried, and only air with the aerosol could be injected into the chamber of the exposed group. In turn, exposed air was removed through the outlet tubing. The mice were exposed with or without the ammonium nitrate/sulfate mixture aerosol for 5 h per day with limited access to food and water, for 7 consecutive days. A solution with ammonium sulfate and ammonium nitrate was used at a concentration of 50 mM (about 50 mg/m^3 in the air). To determine the concentration of the exposure, Scanning Mobility Particle Sizer (SMPS) (Model 3080, TSI, USA) and Condensation Particle Counter (CPC) (Model 3776, TSI, USA) were equipped at the inlet and outlet tubing of the chambers with particles measured in a range of 1–700 nm, which showed 50 mg/m^3 in the chamber. For the range of 1–10 μm, devices with the light scattering method (QABE002-HYK, WINIX) showed 150 μg/m^3 in the chamber, which has been considered appropriate aerosol concentration according to previous studies conducting PM exposure experiment to mouse model (Cory-Slechta et al., 2019; Jew et al., 2019; S.Y. Kim et al., 2019; Yang et al., 2012). After the experiment, mice from the exposed and unexposed groups were sacrificed, and the lung tissues were prepared rapidly and frozen in liquid nitrogen. These tissues were subsequently homogenized, and total RNAs were extracted with TRIzol. For the immunostaining of the tissue, mice from each group were perfused with cold 0.1 M PBS and 4% PFA (SIGMA) dissolved in 0.1 M PBS subsequently. For fixation, the prepped tissue was incubated in 4% PFA for 12 h and then in 30% sucrose for 24 h. After fixation, tissue samples were cut into 45 μm-thick sections with a sliding microtome (SM2010R, Leica).

2.13. Statistical analysis

Statistical analyses for cell viability test and RT-qPCR were performed using Microsoft Excel 2016 software for one-tailed *t*-test with unequal variance. For multiple group testing, ANOVA followed by Tukey's HSD test was performed using R v4.0.3. All data are presented as the mean ± s.e.m. as indicated in the figure legends. A P-value < 0.05 was considered as statistically significant (*P < 0.05, **P < 0.01, ***P < 0.001). The sample size *n* is presented in the figure legends. Statistical analyses for RNA sequencing data were performed as specified in the method section "RNA Sequencing Library Preparation and Data Processing."

3. Results

3.1. Characterization of the PM particles

The size distribution and ion concentrations of the two model PMs, Diesel PM and Fine Dust, are shown in Fig. 2A and B. The hydrodynamic diameter of the Diesel PM in water ranges from 80 to 1300 nm and that of Fine Dust ranges from 150 to 6000 nm. In the case of the Fine Dust, large sedimenting particles existed and were removed before the DLS analysis to avoid interference during the measurement. The average size of the Diesel PM is slightly larger in the buffer than in water, which might be occurred due to the aggregation of the charged diesel exhaust particles in the presence of salt ions in the buffer (Maricq, 2006). The concentrations of the five most dominant species of PM, SO_4^{2-}, NO_3^-, NH_4^+, Na^+, and Cl^-, were analyzed. Other ions of PM were ignored because based on the analysis of water-soluble species of PM in previous studies (Karthikeyan and Balasubramanian, 2006; Shon et al., 2012; Son et al., 2012), the concentrations of other ions were expected to be lower than the detection limit of IC under our experimental condition. As shown in the IC measurement (Fig. 2B), Fine Dust collected from a road tunnel contained more ionic components except for the ammonium ion. The mass fractions of the Fine Dust were comparable to the values in the literature using the same materials (ERM-CZ100 and ERM-CZ120) as ours (ERM-CZ100), indicating that our analysis is reliable (Emma et al., 2018).

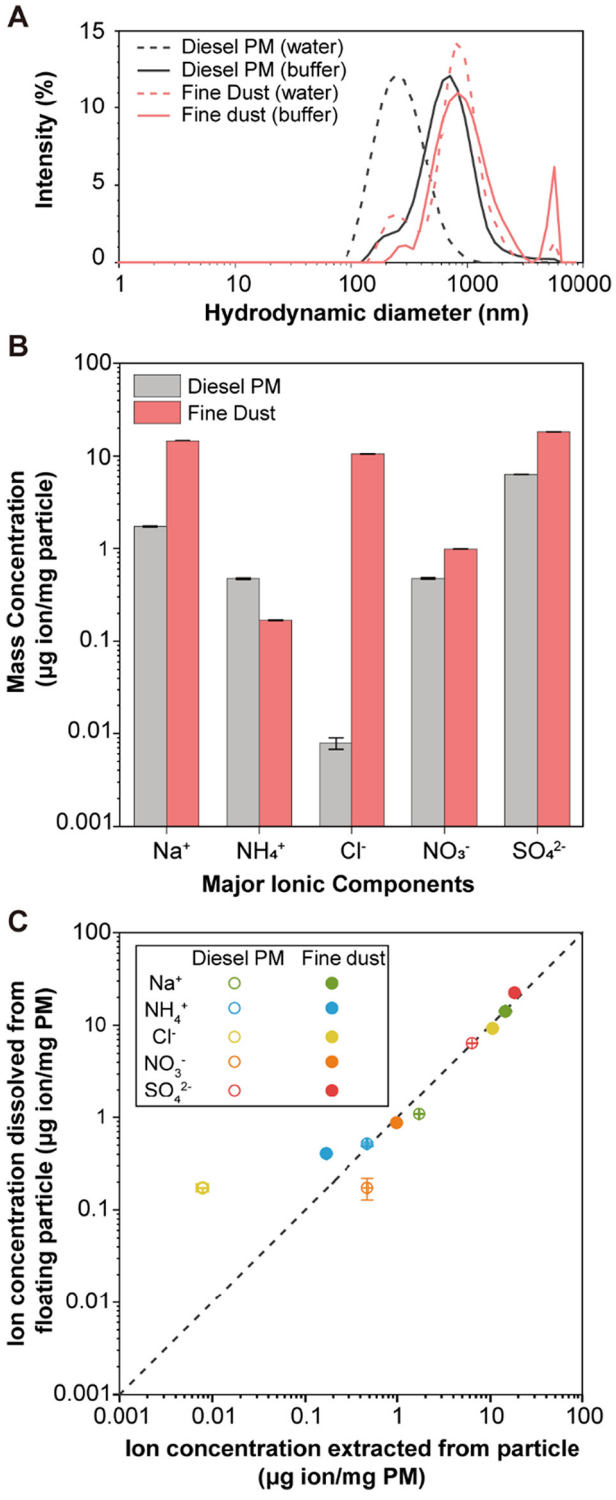

Fig. 2. Characteristics of Diesel PM and Fine Dust used in this study and penetration of inorganic ions in the particles through the model lung surfactant layer. (A) Hydrodynamic size distribution of the Diesel PM (gray) and Fine Dust (red) in water (dashed line) and buffer (solid line). (B) Mass concentrations of the major inorganic ions (Na^+, NH_4^+, Cl^-, NO_3^- and SO_4^{2-}) in the Diesel PM (gray) and Fine Dust (red) ($n = 3$). (C) A plot of the ion mass concentration of the particles *versus* ion mass concentration dissolved from the particles floating at the surfactant-laden air/water interface into the aqueous subphase. Concentrations of the Na^+ (Green), NH_4^+ (blue), Cl^- (yellow), NO_3^- (orange), and SO_4^{2-} (red) are marked for the Diesel PM (empty circle) and Fine Dust (filled circle), respectively ($n = 3$). The Gray dotted line is a diagonal reference line, y = x.

3.2. Water-soluble ions permeate the surfactant layer

Because the alveolar lining fluid is covered with the lung surfactants, the inhaled particles must contact this surfactant layer, and then the particle itself or specific components of the particle have to penetrate the layer to affect the lungs (Wang et al., 2020). We first studied the behavior of the particles after their adsorption at the surfactant-laden air/water interface to quantitatively study the desorption process (SI text, Figs. S2 and S3). The number of particles at the air/water interface was reduced over all particle size ranges due to the translocation from the interface to the aqueous subphase after repeated compression/expansion cycles (Fig. S3C to E) as observed in previous reports (Geiser et al., 2003; Schürch et al., 1990). However, a considerable fraction of particles remained at the interface (56% by area concentration of particles at the interface) even after several compression and expansion cycles (SI text, and Fig. S3E).

To evaluate the penetration of major ions from the inhaled PM into the alveolar region, ion concentrations of the aqueous subphase onto which lipids and particles were spread were measured and compared with the ionic composition of the particles themselves. The x-axis in Fig. 2C is an intrinsic mass concentration of the ions in the particle, which is the same as the values in Fig. 2B, and the y-axis is the dissolved amount from the floating particle analyzed from the collected subphase. As shown in the figure, almost all data points are located near the diagonal line, which signifies that the concentration of dissolved ions from the particle is the same as the concentration of ions in the particle itself. Therefore, we concluded that once the particles are adsorbed at the air/water interface, almost all the ions in the particle dissolve into the aqueous subphase within 24 h. Errors at low ion concentrations might arise from the analytical limit near the detection threshold of the IC measurement. Overall, our results indicate that once the particle is deposited into the alveolar region, the water-soluble ionic components of the particles mostly dissolve into the aqueous environment, passing through the surfactant layer at the air/water interface and can affect alveolar cell function directly.

3.3. Ammonium salts exposure affects gene expression globally

Following the permeation experiment of ions of PM, we subsequently questioned whether major water-soluble salts, ammonium nitrate and sulfate, could affect the cellular metabolism in lung epithelial cells. To find an adequate concentration for the ammonium salt treatment, we first treated A549 lung adenocarcinoma cells with different concentrations of ammonium nitrate or ammonium sulfate for 2 days and measured the cell viability to determine the 50% inhibitor concentration (IC50) (Fig. 3A; nitrate, IC50 = 10.22 mM and sulfate, IC50 = 5.26 mM). Then, to examine the molecular alteration at a genome-wide level, we performed RNA sequencing of the A549 cells treated with media-only (Control) or ammonium salts at a concentration near the IC50 (10 mM nitrate, Nit; 5 mM sulfate, Sul; or 5 mM nitrate/sulfate mixture in 1:1 ratio, Mix) (Fig. 3B). We found that many genes were differentially expressed by the exposure to inorganic salts when compared to the control (Fig. 3C). Among 12,909 expressed genes, we found a total of 1541 DEGs ($|\log_2$ fold change $> 1.5|$ and P-value < 0.01). Individually, when compared to the control, we found 649 DEGs for the ammonium nitrate (Nit), 790 DEGs for the ammonium sulfate (Sul), and 1334 DEGs for the ammonium nitrate/sulfate mixture (Mix). To test the specificity of the DEGs, we examined the list of overlapped DEGs using an upset plot and found that most DEGs were identified in all three cases (Fig. 3C). To our surprise, the majority of the DEGs, even more than the overlapped DEGs, were specific to the response for the ammonium nitrate/sulfate mixture treatment (Fig. 3C). Moreover, while the transcriptome expression profile of the DEGs showed a similar expression pattern among the three different conditions, a stronger magnitude of differential expression was induced by the ammonium nitrate/sulfate mixture treatment (Fig. 3D). This genome-wide analysis indicates a similarity between the responses by ammonium nitrate and sulfate, as well as an interactive effect between the two in the mixture.

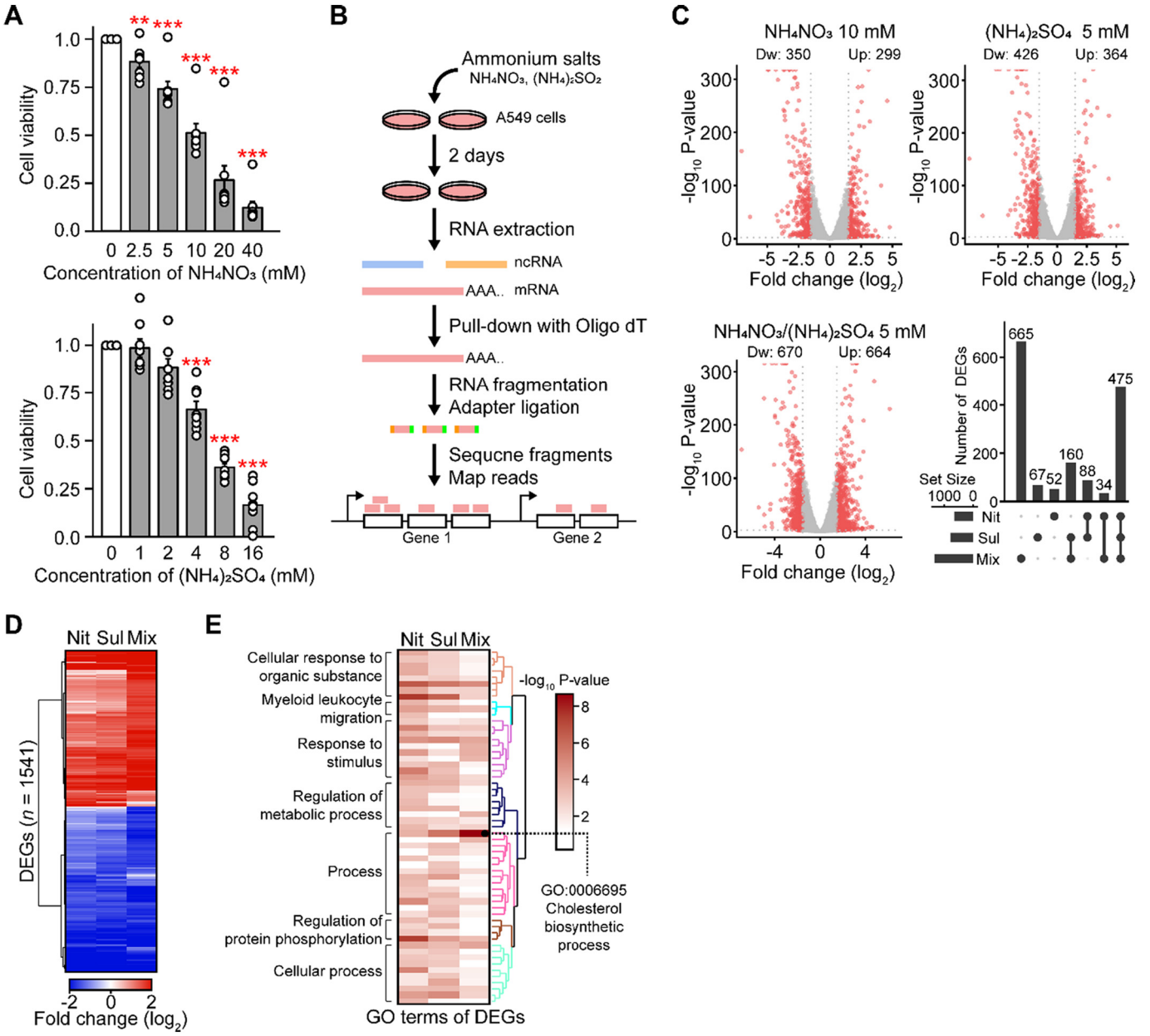

Fig. 3. Genome-wide RNA sequencing analysis of A549 cells treated with ammonium nitrate or sulfate for 2 days. (A) Cell viabilities of A549 cells treated with media-only (Control) or ammonium salts (10 mM nitrate or 5 mM sulfate) for 2 days ($n = 8$). The average is shown with error bars indicating the s.e.m. (B) Schematic of the genome-wide RNA sequencing to investigate the effect of exposure to ammonium nitrate and sulfate on A549 cells. (C) RNA sequencing analysis of A549 cells treated with media-only (Control) or ammonium salts (10 mM nitrate, 5 mM sulfate, or 5 mM nitrate/sulfate mixture) for 2 days. The volcano plots show the fold change and the statistical significance of genes with DEGs indicated in red. The numbers of up or downregulated DEGs are specified. The right-bottom upset plot summarizes the number of DEGs with the number of DEGs specified on the bar. (D) Heat map showing the fold change of the DEGs in the A549 cells treated with media-only (Control) or ammonium salts (10 mM nitrate, 5 mM sulfate, or 5 mM nitrate/sulfate mixture) for 2 days. (E) Heat map and hierarchical clustering for enriched GO terms from the DEGs of (d). GO terms in the same cluster are indicated with the same color, and their ancestor GO terms are specified on the left. (*) $P < 0.05$, (**) $P < 0.01$, (***) $P < 0.001$. Statistical significances were calculated using one-tail Student's *t*-tests.

To capture the biological significance of the DEGs, the enrichment of Gene Ontology (GO) terms in the DEGs were analyzed using Fisher's exact test with the *weight01* algorithm and GO annotation from the Ensembl database (Fig. 3E). In the human GO Release 104, the enrichment tests revealed 57 GO terms for the three treatment conditions. Because the GO term analysis has a limitation due to the overrepresentation of GO terms sharing similar gene components, we used a clustering heat map plot of the GO terms based on semantic similarity (SS) to interpret the biological meaning (Fig. 3E). The GO term enrichment profile of the A549 cells in the different ion treatment conditions resembled each other as in the case of the transcriptome profile. However, we found some GO terms, such as GO:0006695 (Cholesterol biosynthetic process), were more significant in the mixture condition compared to those of the ammonium nitrate or ammonium sulfate condition alone, which reaffirms the synergistic effect of the mixed ammonium salts.

To further analyze this synergistic effect, we checked the list of overlapped GO terms and found three GO terms, including the glycolysis pathway (Fig. S5). To validate our analysis, we performed GSEA with predefined Hallmark gene sets. Consistent with the GO term analysis, we found that genes for cholesterol homeostasis and glycolysis pathway were significantly upregulated (Fig. S6). Altogether, our results demonstrate that water-soluble ions such as ammonium salts affect the transcriptome

profile and influence key biological processes such as cholesterol metabolism. Moreover, the unique DEGs specific to the ammonium nitrate and sulfate mixture and the following GO term analysis and GSEA suggest a synergistic effect between PM components.

3.4. Ammonium salts exposure enhances the neutral lipid metabolism

To validate our RNA sequencing analysis, we used RT-qPCR and analyzed the gene expression changes for several selected genes (*LSS*, *TM7SF2*, *INSIG1*, *HMGCR*, and *ABCG1*) from the key GO term GO:0006695 featured in Fig. 3E (Fig. 4, A and B). In addition, we confirmed the synergistic effect resulting in a greater magnitude of RNA expression change in the ammonium nitrate/sulfate mixture condition compared to the other ion treatment conditions (Fig. 4B). To test the molecular phenotype from the changes in the transcriptome, we further investigated whether the increased gene expression was reflected in the production and subsequent accumulation of cholesterol inside the cells. To visualize the cholesterol, we stained the cells using a fluorescent dye with a high affinity for neutral lipid droplets. Consistent with our gene expression analysis, we found that exposure to ammonium nitrate and sulfate led to the accumulation of neutral lipid droplets in the cells (Fig. 4C). While examining the phase-contrast images, we observed that the accumulated neutral lipids were colocalized with unknown vesicles in the cytosol. We then examined whether other lipids were also upregulated and accumulated in the cells when treated with nitrates and sulfates. We found that the phospholipids did not accumulate in the cells and that their localization did

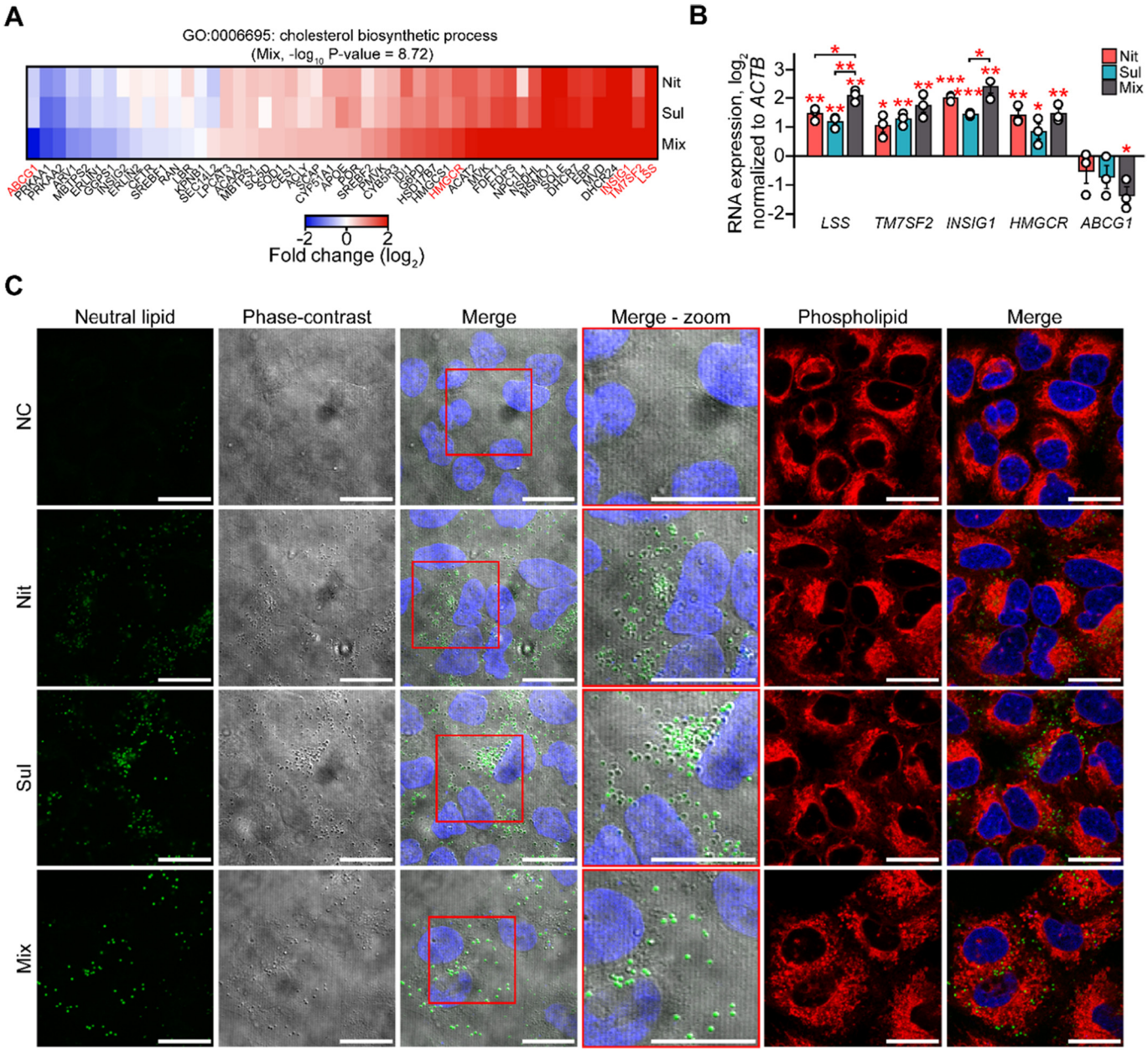

Fig. 4. Ammonium nitrate and sulfate accumulate neutral lipids in cells. (A) Heat map showing fold change of the genes listed in GO:0006695 (cholesterol biosynthetic process). Representative genes are marked in red. (B) RT-qPCR analysis showing relative expression levels of the genes marked in red in panel (A) normalized to the housekeeping gene (*ACTB*) in A549 cells treated with media-only (Control) or ammonium salts (10 mM nitrate, 5 mM sulfate, or 5 mM nitrate/sulfate mixture) for 2 days ($n = 3$). The average is shown with error bars which indicate the s.e.m. (C) Confocal images of neutral lipid or phospholipid stained A549 cells treated with media-only (NC) or ammonium salts (10 mM nitrate, 5 mM sulfate, or 5 mM nitrate/sulfate mixture) for 2 days. Scale bars indicate 20 μm. (*) $P < 0.05$, (**) $P < 0.01$, (***) $P < 0.001$. Statistical significances were calculated using ANOVA followed by Tukey's HSD tests.

not overlap with the newly formed vesicles. Because the dye used in the analysis has specificity toward various types of neutral lipids, accumulated lipids may reflect the increased expression of genes involved in the biosynthesis of neutral lipids in addition to cholesterol. We returned to our RNA-seq data to examine the expression change of the genes involved in the regulation of neutral lipids other than cholesterol. However, none of these gene-sets showed any significant change in expression by exposure to nitrates and sulfates (Fig. S7). Therefore, our data show that exposure to two major anions of PM can alter the gene expression globally at the transcriptional level, which is translated to specific molecular phenotypes such as the accumulation of cholesterol.

3.5. PM exposure induces oncogene expression

As the ammonium nitrate and sulfate treatments perturbed the global transcriptome, we further investigated whether water-soluble ions treatment may drive key PM-associated human diseases, especially lung cancer (Hoek et al., 2013; Kim et al., 2015; Valavanidis et al., 2008; World Health Organization, 2016). While the oncogenes involved in lung cancer are well identified, the contribution of the lung cancer oncogenes during PM exposure is yet unknown. To uncover the association of lung cancer and the gene expression regulation by the ammonium nitrate and sulfate treatment, we performed GSEA on the previously identified putative lung cancer oncogenes (Li et al., 2006). We obtained a list of lung cancer oncogenes and examined their expression in A549 cells treated with ammonium nitrate/sulfate mixture compared to those in cells treated with media-only (Control). These lung cancer oncogenes were identified by transcript, genomic microarray, and proteomics analyses in several lung adenocarcinoma cell lines relative to normal bronchial epithelial cell lines (Li et al., 2006). We examined three gene-sets of lung cancer oncogenes from this study: 1) genes with a significantly increased mRNA level; 2) genes with an increased DNA copy number that correlates with an increased RNA expression and 3) proteins showing significant overexpression in lung cancer cell lines relative to normal bronchial epithelial cell lines. Our GSEA revealed statistically significant enrichment with a normalized enrichment score (NES) of 1.91, 2.14, and 2.06, respectively (Fig. 5). These results support the potential oncogenic effect of PM exposure (Hoek et al., 2013; Kim et al., 2015; Valavanidis et al., 2008; World Health Organization, 2016) at the gene expression level.

3.6. Genome-wide profiling of the molecular effects of moderate-dose exposure to the ammonium salts

Our RNA-sequencing analysis depicts the genome-wide changes in gene expression induced by the key components of PM and reveals the potential oncogenic effect of PM exposure. However, our analysis was conducted near the IC50 value of the nitrate and sulfate ions which might be unphysiologically high. To determine the adequate and relevant exposure condition, the range of alveolar concentrations of PM-derived ions was deduced with some additional assumptions (SI text). First, we assumed that a person is exposed to PM for 1 h per day; second, inorganic ions comprise 30% of the PM2.5 mass (Son et al., 2012); third, 30% of the inhaled particles deposits deep in the lungs (Koullapis et al., 2018); and fourth, the adsorbed particles remain inside the alveoli for a day. Under these conditions, when the ambient PM2.5 concentration is 25 $\mu g/m^3$ (a daily threshold mean value from the WHO air quality guidelines (World Health Organization, 2016)), the calculated alveolar ion concentration is on the order of 1 μM.

We then investigated whether this physiologically relevant concentration of PM exposure still resulted in significant changes in gene expression. We first examined the cell viability upon moderate PM exposure. Even though the concentrations of PM exposure were much lower than the IC50 values measured in Fig. 3A, we still observed a moderate inhibition of cell proliferation (Fig. S8A). We then performed RNA sequencing of the cells treated with a range of concentrations around the predicted concentration of 1 μM (from 10 nM to 100 μM). We found that treating cells with a concentration of 10 μM or higher of the nitrate/sulfate mixture resulted in a significant number of DEGs with specific GO enrichment (Fig. 6, A and B and Fig. S8B). This RNA sequencing result indicates that the critical concentration, above which significant gene expression changes and subsequent alternation in cellular homeostasis may occur, is between 1 and 10 μM for the ammonium nitrate/sulfate mixture.

Next, we examined the oncogenic effect of the exposure to moderate concentrations of the nitrate/sulfate mixture. Though a weaker significance compared to the result for the extreme PM exposure, GSEA still supported the positive enrichment of lung cancer oncogenes (Fig. 6C and Fig. S9). We also examined cholesterol homeostasis and glycolysis, two key changes by high-dose exposure to nitrate and sulfate ions, and found upregulation in the expression of most of the genes involved in these processes (Fig. S10). Of note, despite the upregulation, the overall NESs were still negative, which may be due to insufficient differential fold changes in the gene expression. Altogether, these results support that a moderate concentration of PM over 1 μM can still result in significant perturbation in gene expressions to affect the overall cellular metabolism.

Next, we asked whether the composition of PM components affects the biological effect of the PM exposure at the physiological concentration. We performed RNA sequencing with A549 cells treated with media-only (Control) or ammonium nitrate/sulfate mixture of various concentration ratios for 2 days (Fig. S11). We found that near the physiological concentration, treatment of ammonium sulfate showed more substantial effects on the transcriptome profile than that of ammonium nitrate. Interestingly, the ammonium salts mixture showed non-average but unique responses from

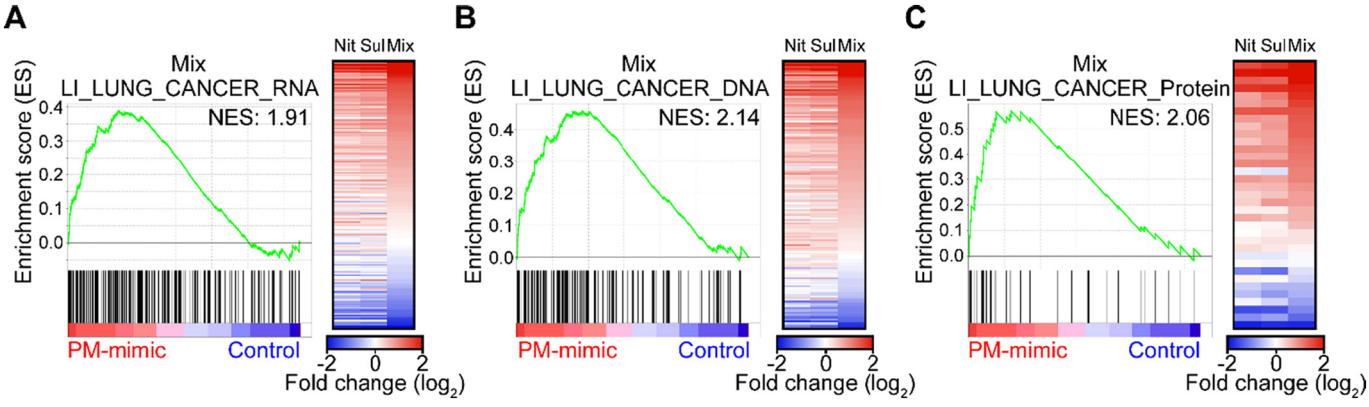

Fig. 5. Oncogenic effect of ammonium nitrate and sulfate. GSEA on the previously identified lung cancer oncogenes with (A) significantly increased mRNA levels in lung cancer cell lines relative to normal bronchial epithelial cell lines or (B) increased DNA copy number that correlates with increased expression across human lung cell lines or (C) the proteins showing significant overexpression in lung cancer cell lines relative to normal bronchial epithelial cell lines in A549 cells treated with 5 mM ammonium nitrate/sulfate mixture for 2 days. The heat map on the right shows the fold change of the genes used in the GSEA.

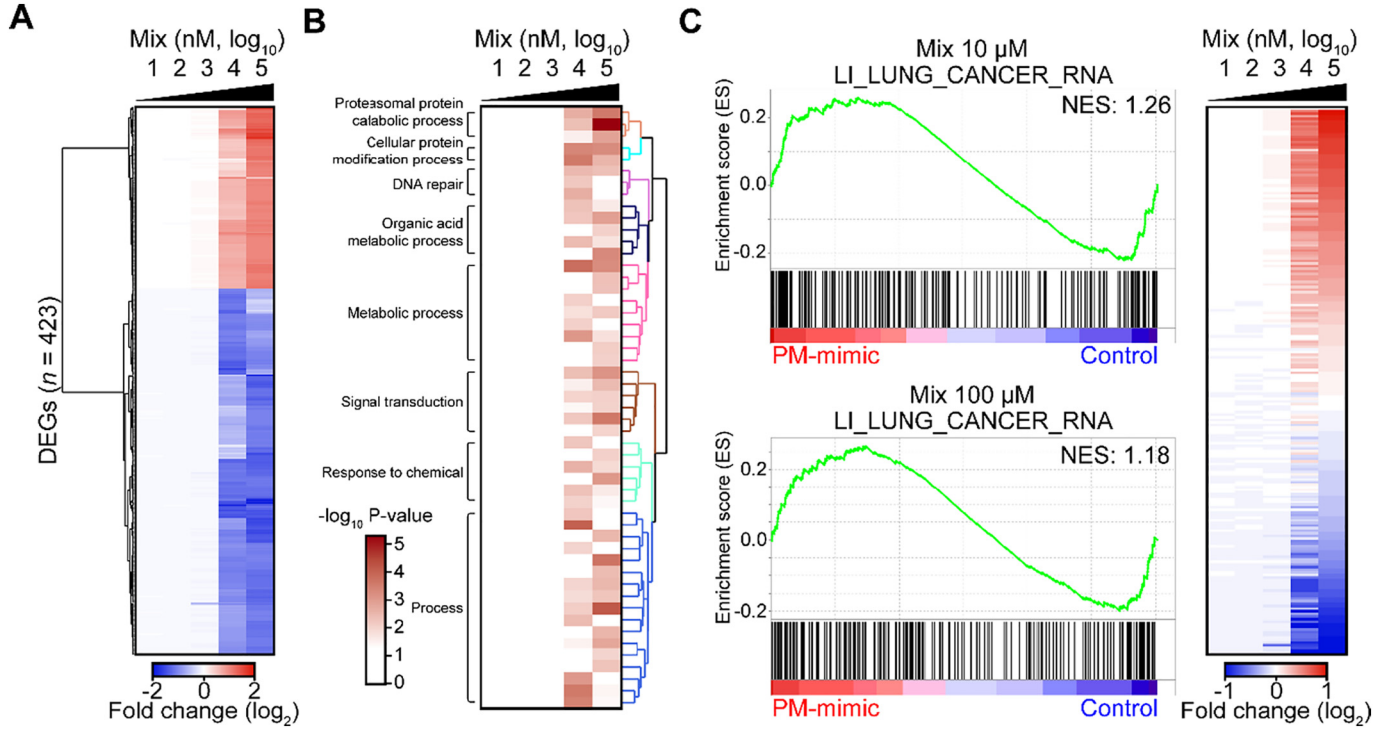

Fig. 6. Genome-wide RNA sequencing analysis of A549 cells treated with moderate concentrations of the ammonium nitrate/sulfate mixture for 2 days. (A) Heat map showing fold change of DEGs in A549 cells treated with media-only (Control) or a moderate concentration of the ammonium nitrate/sulfate mixture for 2 days. (B) Heat map and hierarchical clustering for enriched GO terms from DEGs in A549 cells treated with media-only (Control) or a moderate concentration of the ammonium nitrate/sulfate mixture for 2 days. GO terms in the same cluster are shown with the same color, and their ancestor GO terms are specified on the left. (C) GSEA on the genes with significantly increased mRNA levels in lung cancer cell lines relative to normal bronchial epithelial cell lines in A549 cells treated with 10 μM (top) or 100 μM (bottom) of the ammonium nitrate/sulfate mixture for 2 days. The heat map on the right shows the fold change of the genes used in the GSEA.

those of individual ammonium salts. Overall, these indicate that the composition of PM is important to the molecular effects of PM exposure, which further suggests the potential interactive effects among not only water-soluble inorganic ions but also different toxic PM components, such as heavy metals, may exist.

3.7. Ammonium salts activate immune responses in the mouse lung

To investigate the *in vivo* relevance of our findings, we analyzed the gene expression changes in lung tissues of mice exposed to PM particles. Indeed, the mouse lung model has been used to study the behavior of the lung dynamics, including particle deposition, pathogenesis, and clinical effects (Li et al., 2019; Maes et al., 2010; Miller and Spence, 2017). To expose the particles of the ammonium nitrate/sulfate mixture to mice, we built a customized cage that was connected to a particulate generator. Briefly, air, including particles from the ammonium nitrate/sulfate mixture, was generated by a particulate generator and provided inorganic salts as a form of aerosol to the mice for 5 h per day for 7 consecutive days. We extracted total RNAs from the lungs of mice exposed to aerosols and performed RNA sequencing (Fig. 7A). We found 166 DEGs in the lung tissues of the aerosol exposed mice compared to those in the non-exposed controls (Fig. 7B). We then examined the oncogenic effect of the exposure to the nitrate/sulfate mixture in the mouse lung model. Consistent with the result of the *in vitro* experiments, GSEA showed that the lung cancer oncogenes were highly upregulated (Fig. 7C and Fig. S12A and B). Of note, the GO term analysis did not show terms related to the cholesterol biosynthetic process due to the low fold change while the GSEA analysis of cholesterol homeostasis showed enrichment with an NES of 0.93 (Fig. S12C).

One key difference between our *in vitro* experiments and lung tissue analysis is that the latter contained different types of cells. Interestingly, the GO term analysis revealed the potential involvement of leukocyte recruitment into the lung tissue by the aerosol exposure (Fig. 7D). For example, gene expression of the CC chemokine receptor or ligand such as Ccr6 or Ccl2 listed in GO:0002523 (Leukocyte migration involved in inflammatory response) was significantly upregulated by the aerosol exposure to the ammonium nitrate/sulfate mixture in mice. Because Ccr6 is expressed on immune cells such as B cells, T cells, natural killer T (NKT) cells, dendritic cells, and neutrophils (Schutyser et al., 2003), and Ccl2 recruits monocytes, memory T cells, and dendritic cells to the sites of inflammation produced by tissue injury or infection (Carr et al., 1994; Deshmane et al., 2009; Xu et al., 1996), our transcriptome analysis indicates the possible recruitment of immune cells into the lungs. Using the molecular atlas profiled by Travaglini et al. (Travaglini et al., 2020), we examined whether the immune cells were recruited in the lung tissue upon exposure to the nitrate/sulfate mixture aerosol (Fig. 7E). The GSEA for cell-type identification revealed the induction of marker genes for several lymphocytes, including B cells, proliferating NKT cells, and CD4 memory effector T cells in the mouse lung tissues exposed to the ammonium nitrate/sulfate mixture aerosol. We further performed GSEA and found that genes for the inflammatory response were significantly enriched in the lung tissue of mice. (Fig. 7F). In particular, interferon-gamma (IFNγ) production was induced in the lungs of mice under nitrate/sulfate exposure, which is consistent with the enrichment of marker genes for NK cells, NKT cells, B cells, and antigen-presenting cells (macrophage, dendritic cells) as these cells are known to secrete IFNγ (Schroder et al., 2004) (Fig. 7F). In addition to the production, GSEA for response to IFNγ showed strong enrichment in mouse lungs (Fig. S13). At the same time, the production of interferon-alpha (IFNα) and -beta (IFNβ) and response to IFNα and IFNβ were not significant. Collectively, our analyses indicate that the observed IFNγ production is specific.

To validate our RNA sequencing analysis on the signatures for leukocyte migration and IFNγ, we used RT-qPCR to analyze the gene expression changes (Fig. 4G). Exposure to ammonium nitrate/sulfate mixture aerosol induced upregulation in gene expression of most genes involved in

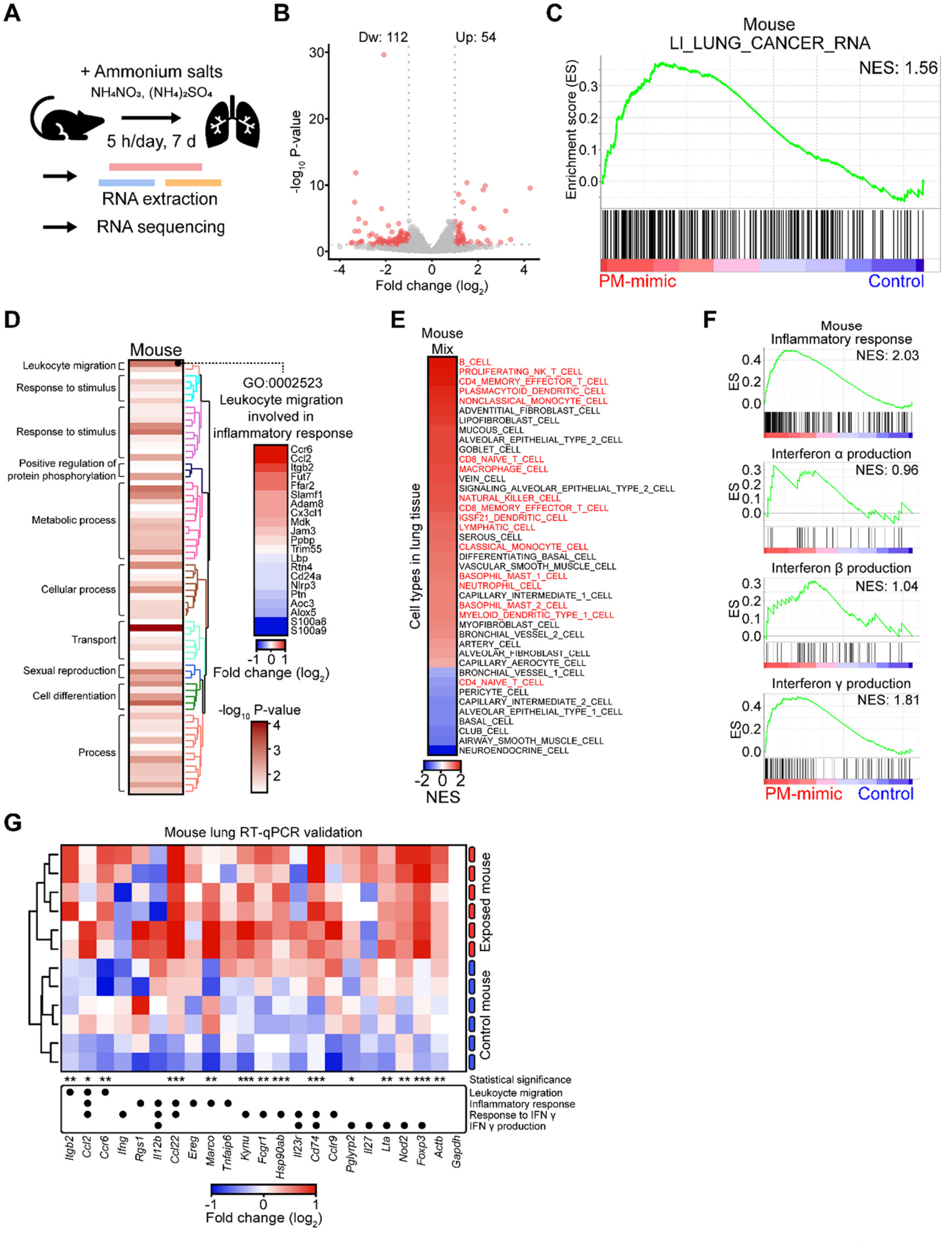

(caption on next page)

leukocyte migration or IFNγ signatures. Considering that IFNγ is mainly produced by several lymphocytes and associated with leukocyte attraction whereas IFNβ is secreted by epithelial fibroblasts (Schroder et al., 2004), the observed IFNγ signature strongly supports the activation of the immune system in response to the aerosol exposure of the nitrate/sulfate mixture.

4. Discussion

Exposure to ambient PM significantly affects human respiratory health. However, the current understanding of the health hazard of PM exposure is limited due to the diverse physical and chemical characteristics of PM. This study provides clues to elucidate the relationship between PM and respiratory health at the molecular level, particularly by the water-soluble inorganic ions of PM. Using the lung surfactant layer to mimic the pulmonary surfactants of the lungs, we show that a considerable amount of inhaled particles is blocked by the surfactant layer, but water-soluble inorganics, such as nitrate and sulfate ions, can entirely permeate the surfactant layer covering the air/water interface within a day. Consistent with our findings, several *in vivo* experiments showed that the inhaled particles were present inside the alveoli even 24 h after inhalation prior to the particle clearance process (Geiser and Kreyling, 2010; Sorokin and Brain, 1975; Yang et al., 2008).

The water-soluble components can be dissolved into the aqueous surroundings during particle retention in the alveolar region, so it is essential to understand the health impacts of the permeated ionic components of PM. Using RNA sequencing, we evaluated the genome-wide effects of the permeated water-soluble ions to uncover the detailed molecular effects of PM exposure. Interestingly, treatment of individual ammonium nitrate or sulfate salt showed similar transcriptome profile patterns whereas the treatment of a mixture of the two resulted in unique gene expression changes, indicating a possible interactive effect among the components of PM. Moreover, our analysis revealed that exposure to nitrate and sulfate ions changes the cellular metabolism, such as the cholesterol biosynthetic process, and induces oncogenic gene expressions. Enrichment of markers of the immune cells in the lungs of mice exposed to aerosols of the nitrate/sulfate mixture further supported the *in vivo* relevance of our findings.

Our results provide a potential roadmap in understanding the human health hazard imposed by PM exposure at a molecular level. Recently, several studies also used next-generation sequencing (NGS) for a non-biased genome-wide assessment upon ambient PM exposure (Kang et al., 2020; Park et al., 2021). They identified mutational signatures and DEGs associated with lung cancer in PM10 exposed lung cancer cell lines. In the current study, we further provided experimental verification of the changes induced by the exposure to inorganic ions. Moreover, by analyzing human lung adenocarcinoma cells and mouse lungs both exposed to the ammonium nitrate/sulfate mixture in parallel, we were able to identify key common signatures of PM exposure such as the activation of cholesterol metabolism and the induction of oncogenes. Lastly, using the mouse lung model, we found IFNγ-associated immune response and immune cell recruitment to the exposed lungs.

The activation of cholesterol metabolism by ammonium nitrate and sulfate suggests one possible mechanism that may account for the oncogenic effects of PM exposure. Cholesterol-derived metabolites can induce tumorigenesis and cancer progression by modifying signaling proteins such as Hedgehog and Smoothened (Porter et al., 1996; Xiao et al., 2017). Indeed, accelerated cholesterol metabolism is one of the hallmarks of many types of cancer (Huang et al., 2020; Snaebjornsson et al., 2020). Consistent with this, our analysis also revealed that the genes previously implicated to have oncogenic effects in lung adenocarcinoma (Li et al., 2006) were highly upregulated when cells were exposed to the ammonium nitrate/sulfate mixture. Similar molecular effects were observed in mouse lungs exposed to the aerosols of the nitrate/sulfate mixture. In addition, cholesterol metabolites can also modulate the immune system by inhibiting immune-effector cells, interfering with antigen presentation, and interacting with immunosuppressive cells, resulting in their enrichment in the microenvironment (Huang et al., 2020). Consistent with this, our analysis also clearly showed the potential recruitment of immune cells into the lung tissues exposed to inorganic aerosols through increased production of IFNγ. Currently, the exact nature of cholesterol-derived metabolites induced by PM exposure is unclear due to a lack of methodology to examine the chemical composition of the accumulated neutral lipid droplets. Based on the findings of our study, we expect that screening for cholesterol-derived metabolites may provide the appropriate target to prevent or alleviate the health hazard of PM exposure.

One of the important findings of this study is that the mixture of the two major inorganic ions of ambient PM has unique molecular effects that cannot be explained by analyzing the effects of nitrate and sulfate ions independently. Although additional analysis is required, our result suggests that the PM-associated health hazard may depend on the chemical composition of the inhaled PM. Considering an earlier study that reported different toxicities of PM derived from different sources (Park et al., 2018), assessing the contribution of individual components of PM and their synergistic effects will be necessary to fully understand the health threats imposed by PM and to devise appropriate regulations. Altogether, our results suggest that the chemical composition of PM is an important factor for the health hazard imposed by ambient PM exposure.

Despite the important findings on the potential health impacts of the inorganic ions in PM, this study has limitations. PM also contains other toxic species such as polycyclic aromatic hydrocarbons (PAHs) and heavy metals. Considering their notable contribution to the health hazard, exploring the interactive effects between those hazardous substances with inorganics will be essential. In addition, the temporal and spatial variations in the size and chemical composition of PM and the size-dependent lung deposition of the inhaled particles need to be considered along with the penetration of the ionic species into the alveolar region.

5. Conclusion

This study suggests water-soluble inorganic ions, such as nitrates and sulfates, as a potential source of PM-mediated toxicity. The water-soluble ionic components of PM particles can rapidly penetrate the surfactant layer in the lungs. The activation of cholesterol biosynthetic metabolism and tumorigenesis in lung adenocarcinoma cells exposed to nitrate and sulfate ions suggests the oncogenic effects of PM exposure. The inorganics also induce IFNγ-associated immune response in the mouse lung tissues. Moreover, the mixtures of sulfates and nitrates synergistically perturb the gene expressions. Collectively, our results provide clues for understanding the effects of PM exposure on human health at a molecular level.

← **Fig. 7.** Genome-wide RNA sequencing analysis of lung tissues of mice exposed to the ammonium nitrate/sulfate mixture. (A) Schematic of the genome-wide RNA sequencing to investigate the effect of exposure to ammonium salts in mice. (B) Volcano plot showing the fold change and the statistical significance of genes in the lung tissue of mice exposed to the ammonium nitrate/sulfate mixture ($n = 2$) where DEGs are indicated in red. (C) GSEA on the genes with significantly increased mRNA levels in lung cancer cell lines relative to normal bronchial epithelial cell lines. (D) Heat map and hierarchical clustering for enriched GO terms from DEGs in lung tissue of mice exposed to the ammonium nitrate/sulfate mixture. (E) Heat map showing the NES of the gene sets of the enriched cell type marker genes in mouse lung tissue exposed to the ammonium nitrate/sulfate mixture in ascending order of NES. Immune cell types are marked in red. (F) GSEA on the genes listed in the Hallmark gene sets of inflammatory response and interferon α, β, and γ production in lungs of mice exposed to the ammonium nitrate/sulfate mixture. (G) RT-qPCR analysis showing relative expression levels of genes involved in leukocyte migration or IFNγ signatures normalized to the housekeeping gene (*Gapdh*) in lung tissues of mice exposed to the ammonium nitrate/sulfate mixture ($n = 6$). (*) $P < 0.05$, (**) $P < 0.01$, (***) $P < 0.001$. Statistical significances were calculated using one-tail Student's *t*-tests.

CRediT authorship contribution statement

Sujin Park: Conceptualization, Methodology, Investigation, Visualization, Writing-original draft, Writing-review & editing. **Jayoung Ku**: Conceptualization, Methodology, Investigation, Visualization, Writing-original draft, Writing-review & editing. **Sung-Min Lee**: Conceptualization, Methodology, Investigation, Writing-original draft, Writing-review & editing. **Huiseon Hwang**: Conceptualization, Methodology, Investigation, Writing-original draft, Writing-review & editing. **Namseok Lee**: Conceptualization, Methodology. **Hanul Kim**: Conceptualization, Methodology. **Ki-Jun Yoon**: Conceptualization, Methodology, Supervision, Writing-review & editing. **Yoosik Kim**: Conceptualization, Methodology, Supervision, Writing-review & editing. **Siyoung Q. Choi**: Conceptualization, Methodology, Supervision, Writing-review & editing.

Declaration of competing interest

The authors declare that they have no known competing financial interests or personal relationships that could have appeared to influence the work reported in this paper.

Acknowledgment

We thank T. Lee from the Department of Environmental Science, Hankuk University of Foreign Studies, for providing particle generators and helpful discussions. We also thank Y. Koh from Seoul National University College of Medicine for his help with identifying oncogenes. This work was supported by the KAIST-funded Global Singularity Research Program for 2020 [N11200031].

Appendix A. Supplementary data

Supplementary data to this article can be found online at https://doi.org/10.1016/j.scitotenv.2022.153818.

References

Arick, D.Q., Choi, Y.H., Kim, H.C., Won, Y.Y., 2015. Effects of nanoparticles on the mechanical functioning of the lung. Adv. Colloid Interf. Sci. 225, 218–228. https://doi.org/10.1016/j.cis.2015.10.002.

Beck-Broichsitter, M., Ruppert, C., Schmehl, T., Guenther, A., Betz, T., Bakowsky, U., Seeger, W., Kissel, T., Gessler, T., 2011. Biophysical investigation of pulmonary surfactant surface properties upon contact with polymeric nanoparticles in vitro. Nanomedicine nanotechnologyBiol. Med. 7, 341–350. https://doi.org/10.1016/j.nano.2010.10.007.

Bourdon, J.A., Halappanavar, S., Saber, A.T., Jacobsen, N.R., Williams, A., Wallin, H., Vogel, U., Yauk, C.L., 2012. Hepatic and pulmonary toxicogenomic profiles in mice intratracheally instilled with carbon black nanoparticles reveal pulmonary inflammation, acute phase response, and alterations in lipid homeostasis. Toxicol. Sci. 127, 474–484. https://doi.org/10.1093/toxsci/kfs119.

Brionne, A., Juanchich, A., Hennequet-Antier, C., 2019. ViSEAGO: a bioconductor package for clustering biological functions using gene ontology and semantic similarity. BioData Min. 12, 1–13. https://doi.org/10.1186/s13040-019-0204-1.

Cao, J., Xu, H., Xu, Q., Chen, B., Kan, H., 2012. Fine particulate matter constituents and cardiopulmonary mortality in a heavily polluted Chinese city. Environ. Health Perspect. 120, 373–378. https://doi.org/10.1289/ehp.1103671.

Cao, Y., Jantzen, K., Gouveia, A.C.D., Skovmand, A., Roursgaard, M., Loft, S., Møller, P., 2015. Automobile diesel exhaust particles induce lipid droplet formation in macrophages in vitro. Environ. Toxicol. Pharmacol. 40, 164–171. https://doi.org/10.1016/j.etap.2015.06.012.

Carr, M.W., Roth, S.J., Luther, E., Rose, S.S., Springer, T.A., 1994. Monocyte chemoattractant protein 1 acts as a T-lymphocyte chemoattractant. Proc. Natl. Acad. Sci. U. S. A. 91, 3652–3656. https://doi.org/10.1073/pnas.91.9.3652.

Cory-Slechta, D.A., Sobolewski, M., Marvin, E., Conrad, K., Merrill, A., Anderson, T., Jackson, B.P., Oberdorster, G., 2019. The impact of inhaled ambient ultrafine particulate matter on developing brain: potential importance of elemental contaminants. Toxicol. Pathol. 47, 976–992. https://doi.org/10.1177/0192623319878400.

Davoren, M., Herzog, E., Casey, A., Cottineau, B., Chambers, G., Byrne, H.J., Lyng, F.M., 2007. In vitro toxicity evaluation of single walled carbon nanotubes on human A549 lung cells. Toxicol. Vitr. 21, 438–448. https://doi.org/10.1016/j.tiv.2006.10.007.

Deshmane, S.L., Kremlev, S., Amini, S., Sawaya, B.E., 2009. Monocyte chemoattractant protein-1 (MCP-1): an overview. J. Interf. Cytokine Res. 29, 313–325. https://doi.org/10.1089/jir.2008.0027.

Dwivedi, M.V., Harishchandra, R.K., Koshkina, O., Maskos, M., Galla, H.J., 2014. Size influences the effect of hydrophobic nanoparticles on lung surfactant model systems. Biophys. J. 106, 289–298. https://doi.org/10.1016/j.bpj.2013.10.036.

Emma, G., Snell, J., Charoud-Got, J., Held, A., Emons, H., 2018. Feasibility study of a candidate reference material for ions in PM2.5: does commutability matter also for inorganic matrices? Anal. Bioanal. Chem. 410, 6001–6008. https://doi.org/10.1007/s00216-018-1220-6.

Geiser, M., Kreyling, W.G., 2010. Deposition and biokinetics of inhaled nanoparticles. Part. Fibre Toxicol. 7, 1–17. https://doi.org/10.1186/1743-8977-7-2.

Geiser, M., Schürch, S., Gehr, P., 2003. Influence of surface chemistry and topography of particles on their immersion into the lung's surface-lining layer. J. Appl. Physiol. 94, 1793–1801. https://doi.org/10.1152/japplphysiol.00514.2002.

Han, S.H., Mallampalli, R.K., 2015. The role of surfactant in lung disease and host defense against pulmonary infections. Ann. Am. Thorac. Soc. 12, 765–774. https://doi.org/10.1513/AnnalsATS.201411-507FR.

Harishchandra, R.K., Saleem, M., Galla, H.J., 2010. Nanoparticle interaction with model lung surfactant monolayers. J. R. Soc. Interface 7. https://doi.org/10.1098/rsif.2009.0329.focus.

Hemmingsen, J.G., Møller, P., Nøjgaard, J.K., Roursgaard, M., Loft, S., 2011. Oxidative stress, genotoxicity, and vascular cell adhesion molecule expression in cells exposed to particulate matter from combustion of conventional diesel and methyl ester biodiesel blends. Environ. Sci. Technol. 45, 8545–8551. https://doi.org/10.1021/es200956p.

Hoek, G., Krishnan, R.M., Beelen, R., Peters, A., Ostro, B., Brunekreef, B., Kaufman, J.D., 2013. Long-term air pollution exposure and cardio- respiratory mortality: a review. Environ. Health 12, 43. https://doi.org/10.1186/1476-069X-12-43.

Hu, J., Li, X., Li, M., Shang, Y., He, Y., Liu, H., 2020. Real-time monitoring of the effect of carbon nanoparticles on the surface behavior of DPPC/DPPG Langmuir monolayer. Colloids Surf. B Biointerfaces 190. https://doi.org/10.1016/j.colsurfb.2020.110922.

Huang, B., Song, B.liang, Xu, C., 2020. Cholesterol metabolism in cancer: mechanisms and therapeutic opportunities. Nat. Metab. 2, 132–141. https://doi.org/10.1038/s42255-020-0174-0.

Hwang, S.-H., Lee, J.Y., Yi, S.-M., Kim, H., 2017. Associations of particulate matter and its components with emergency room visits for cardiovascular and respiratory diseases. PLoS One 12, e0183224. https://doi.org/10.1371/journal.pone.0183224.

Jew, K., Herr, D., Wong, C., Kennell, A., Morris-Schaffer, K., Oberdörster, G., O'Banion, M.K., Cory-Slechta, D.A., Elder, A., 2019. Selective memory and behavioral alterations after ambient ultrafine particulate matter exposure in aged 3xTgAD Alzheimer's disease mice. Part. Fibre Toxicol. 16, 1–17. https://doi.org/10.1186/S12989-019-0323-3/TABLES/2.

Kang, D., Jung, I.B., Lee, S.Y., Park, S.J., Kwon, S.J., Park, D.H., Son, J.W., 2020. Particulate matter less than 10 μm (PM10) activates cancer related genes in lung epithelial cells. Inhal. Toxicol. 32, 487–493. https://doi.org/10.1080/08958378.2020.1850936.

Karthikeyan, S., Balasubramanian, R., 2006. Determination of water-soluble inorganic and organic species in atmospheric fine particulate matter. Microchem. J. 82, 49–55. https://doi.org/10.1016/j.microc.2005.07.003.

Kim, K.-H., Kabir, E., Kabir, S., 2015. A review on the human health impact of airborne particulate matter. Environ. Int. 74, 136–143. https://doi.org/10.1016/j.envint.2014.10.005.

Kim, D., Paggi, J.M., Park, C., Bennett, C., Salzberg, S.L., 2019. Graph-based genome alignment and genotyping with HISAT2 and HISAT-genotype. Nat. Biotechnol. 37, 907–915. https://doi.org/10.1038/s41587-019-0201-4.

Kim, S.Y., Lee, D.hye, Park, S., Kim, B.G., Jang, A.S., Oh, S.H., Lee, J.H., Suh, M.W., Park, M.K., 2019. Neuronal and perineuronal changes of cerebral cortex after exposure to inhaled particulate matter. Sci. Rep. 9, 1–9. https://doi.org/10.1038/s41598-019-55956-4.

Koullapis, P.G., Hofemeier, P., Sznitman, J., Kassinos, S.C., 2018. An efficient computational fluid-particle dynamics method to predict deposition in a simplified approximation of the deep lung. Eur. J. Pharm. Sci. 113, 132–144. https://doi.org/10.1016/j.ejps.2017.09.016.

Li, R., Wang, H., Bekele, B.N., Yin, Z., Caraway, N.P., Katz, R.L., Stass, S.A., Jiang, F., 2006. Identification of putative oncogenes in lung adenocarcinoma by a comprehensive functional genomic approach. Oncogene 25, 2628–2635. https://doi.org/10.1038/sj.onc.1209289.

Li, D., Li, Y., Li, G., Zhang, Y., Li, J., Chen, H., 2019. Fluorescent reconstitution on deposition of PM 2.5 in lung and extrapulmonary organs. Proc. Natl. Acad. Sci. U. S. A. 116, 2488–2493. https://doi.org/10.1073/pnas.1818134116.

Liao, Y., Smyth, G.K., Shi, W., 2019. The R package Rsubread is easier, faster, cheaper and better for alignment and quantification of RNA sequencing reads. Nucleic Acids Res. 47. https://doi.org/10.1093/nar/gkz114.

Lippmann, M., Chen, L.-C., Gordon, T., Ito, K., Thurston, G.D., 2013. National Particle Component Toxicity (NPACT) Initiative: integrated epidemiologic and toxicologic studies of the health effects of particulate matter components. Res. Rep. Health. Eff. Inst. (177), 5–13.

Love, M.I., Huber, W., Anders, S., 2014. Moderated estimation of fold change and dispersion for RNA-seq data with DESeq2. Genome Biol. 15, 1–21. https://doi.org/10.1186/s13059-014-0550-8.

Maes, T., Provoost, S., Lanckacker, E.A., Cataldo, D.D., Vanoirbeek, J.A.J., Nemery, B., Tournoy, K.G., Joos, G.F., 2010. Mouse models to unravel the role of inhaled pollutants on allergic sensitization and airway inflammation. Respir. Res. 11, 1–16. https://doi.org/10.1186/1465-9921-11-7.

Maricq, M.M., 2006. On the electrical charge of motor vehicle exhaust particles. J. Aerosol Sci. 37, 858–874. https://doi.org/10.1016/j.jaerosci.2005.08.003.

Maynard, D., Coull, B.A., Gryparis, A., Schwartz, J., 2007. Mortality risk associated with short-term exposure to traffic particles and sulfates. Environ. Health Perspect. 115, 751–755. https://doi.org/10.1289/ehp.9537.

Miller, A.J., Spence, J.R., 2017. In vitro models to study human lung development, disease and homeostasis. Physiology 32, 246–260. https://doi.org/10.1152/physiol.00041.2016.

Mootha, V., Lindgren, C., Eriksson, K.F., et al., 2003. PGC-1α-responsive genes involved in oxidative phosphorylation are coordinately downregulated in human diabetes. Nat. Genet. 34, 267–273. https://doi.org/10.1038/ng1180.

Park, M., Joo, H.S., Lee, K., Jang, M., Kim, S.D., Kim, I., Borlaza, L.J.S., Lim, H., Shin, H., Chung, K.H., Choi, Y.-H., Park, S.G., Bae, M.-S., Lee, J., Song, H., Park, K., 2018. Differential toxicities of fine particulate matters from various sources. Sci. Rep. 8, 17007. https://doi.org/10.1038/s41598-018-35398-0.

Park, S.J., Ku, G.W., Lee, S.Y., Kang, D., Hwang, W.J., Jeong, I.B., Kwon, S.J., Kang, J., Son, J.W., 2021. Analysis of single nucleotide variants (SNVs) induced by exposure to PM10 in lung epithelial cells using whole genome sequencing. Int. J. Environ. Res. Public Health 18, 1–11. https://doi.org/10.3390/ijerph18031046.

Porter, J.A., Young, K.E., Beachy, P.A., 1996. Cholesterol modification of hedgehog signaling proteins in animal development. Science 274, 255–259. https://doi.org/10.1126/science.274.5285.255.

Radiom, M., Sarkis, M., Brookes, O., Oikonomou, E.K., Baeza-Squiban, A., Berret, J.F., 2020. Pulmonary surfactant inhibition of nanoparticle uptake by alveolar epithelial cells. Sci. Rep. 10, 1–14. https://doi.org/10.1038/s41598-020-76332-7.

Saad, S.M.I., Policova, Z., Acosta, E.J., Hair, M.L., Neumann, A.W., 2009. Mixed DPPC/DPPG monolayers at very high film compression. Langmuir 25, 10907–10912. https://doi.org/10.1021/la901250z.

Schroder, K., Hertzog, P.J., Ravasi, T., Hume, D.A., 2004. Interferon-γ: an overview of signals, mechanisms and functions. J. Leukoc. Biol. 75, 163–189. https://doi.org/10.1189/jlb.0603252.

Schürch, S., Gehr, P., Im Hof, V., Geiser, M., Green, F., 1990. Surfactant displaces particles toward the epithelium in airways and alveoli. Respir. Physiol. 80, 17–32. https://doi.org/10.1016/0034-5687(90)90003-H.

Schutyser, E., Struyf, S., Van Damme, J., 2003. The CC chemokine CCL20 and its receptor CCR6. Cytokine Growth Factor Rev. 14, 409–426. https://doi.org/10.1016/S1359-6101(03)00049-2.

Shon, Z.-H., Kim, K.-H., Song, S.-K., Jung, K., Kim, N.-J., Lee, J.-B., 2012. Relationship between water-soluble ions in PM2.5 and their precursor gases in Seoul megacity. Atmos. Environ. 59, 540–550. https://doi.org/10.1016/j.atmosenv.2012.04.033.

Snaebjornsson, M.T., Janaki-Raman, S., Schulze, A., 2020. Greasing the wheels of the cancer machine: the role of lipid metabolism in cancer. Cell Metab. 31, 62–76. https://doi.org/10.1016/j.cmet.2019.11.010.

Son, J.Y., Lee, J.T., Kim, K.H., Jung, K., Bell, M.L., 2012. Characterization of fine particulate matter and associations between particulate chemical constituents and mortality in Seoul,Korea. Environ. Health Perspect. 120, 872–878. https://doi.org/10.1289/ehp.1104316.

Sorokin, S.P., Brain, J.D., 1975. Pathways of clearance in mouse lungs exposed to iron oxide aerosols. Anat. Rec. 181, 581–625. https://doi.org/10.1002/ar.1091810304.

Subramanian, A., Tamayo, P., Mootha, V.K., Mukherjee, S., Ebert, B.L., Gillette, M.A., Paulovich, A., Pomeroy, S.L., Golub, T.R., Lander, E.S., Mesirov, J.P., 2005. Gene set enrichment analysis: a knowledge-based approach for interpreting genome-wide expression profiles. Proc. Natl. Acad. Sci. U. S. A. 102, 15545–15550. https://doi.org/10.1073/pnas.0506580102.

Travaglini, K.J., Nabhan, A.N., Penland, L., Sinha, R., Gillich, A., Sit, R.V., Chang, S., Conley, S.D., Mori, Y., Seita, J., Berry, G.J., Shrager, J.B., Metzger, R.J., Kuo, C.S., Neff, N., Weissman, I.L., Quake, S.R., Krasnow, M.A., 2020. A molecular cell atlas of the human lung from single-cell RNA sequencing. Nature 587, 619–625. https://doi.org/10.1038/s41586-020-2922-4.

Valavanidis, A., Fiotakis, K., Vlachogianni, T., 2008. Airborne particulate matter and human health: toxicological assessment and importance of size and composition of particles for oxidative damage and carcinogenic mechanisms. J. Environ. Sci. Health., Part C Environ. Carcinog. Ecotoxicol. Rev. 26, 339–362. https://doi.org/10.1080/10590500802494538.

Veldhuizen, E.J.A., Haagsman, H.P., 2000. Role of pulmonary surfactant components in surface film formation and dynamics. Biochim. Biophys. Acta - Biomembr. 1467, 255–270. https://doi.org/10.1016/S0005-2736(00)00256-X.

Veldhuizen, R., Nag, K., Orgeig, S., Possmayer, F., 1998. The role of lipids in pulmonary surfactant. Biochim. Biophys. Acta - Mol. Basis Dis. 1408, 90–108. https://doi.org/10.1016/S0925-4439(98)00061-1.

Vranic, S., Garcia-Verdugo, I., Darnis, C., Sallenave, J.M., Boggetto, N., Marano, F., Boland, S., Baeza-Squiban, A., 2013. Internalization of SiO2 nanoparticles by alveolar macrophages and lung epithelial cells and its modulation by the lung surfactant substitute Curosurf®. Environ. Sci. Pollut. Res. 20, 2761–2770. https://doi.org/10.1007/s11356-012-1436-5.

Wang, F., Liu, J., Zeng, H., 2020. Interactions of particulate matter and pulmonary surfactant: implications for human health. Adv. Colloid Interf. Sci. 284, 102244. https://doi.org/10.1016/j.cis.2020.102244.

World Health Organization, 2016. Ambient air pollution: a global assessment of exposure and burden of disease. Clean Air J. 26, 6. https://doi.org/10.17159/2410-972X/2016/v26n2a4.

Wyzga, R.E., Rohr, A.C., 2015. Long-term particulate matter exposure: attributing health effects to individual PM components. J. Air Waste Manag. Assoc. 65, 523–543. https://doi.org/10.1080/10962247.2015.1020396.

Xiao, X., Tang, J.J., Peng, C., Wang, Y., Fu, L., Qiu, Z.P., Xiong, Y., Yang, L.F., Cui, H.W., He, X.L., Yin, L., Qi, W., Wong, C.C.L., Zhao, Y., Li, B.L., Qiu, W.W., Song, B.L., 2017. Cholesterol modification of smoothened is required for hedgehog signaling. Mol. Cell 66, 154–162.e10. https://doi.org/10.1016/j.molcel.2017.02.015.

Xu, L.L., Warren, M.K., Rose, W.L., Gong, W., Wang, J.M., 1996. Human recombinant monocyte chemotactic protein and other c-c chemokines bind and induce directional migration of dendritic cells in vitro. J. Leukoc. Biol. 60, 365–371. https://doi.org/10.1002/jlb.60.3.365.

Yang, W., Peters, J.I., Williams, R.O., 2008. Inhaled nanoparticles-a current review. Int. J. Pharm. 356, 239–247. https://doi.org/10.1016/j.ijpharm.2008.02.011.

Yang, L., Zhou, X., Wang, Z., Zhou, Y., Cheng, S., Xu, P., Gao, X., Nie, W., Wang, X., Wang, W., 2012. Airborne fine particulate pollution in Jinan, China: concentrations, chemical compositions and influence on visibility impairment. Atmos. Environ. 55, 506–514. https://doi.org/10.1016/J.ATMOSENV.2012.02.029.

Zhu, A., Ibrahim, J.G., Love, M.I., 2019. Heavy-tailed prior distributions for sequence count data: removing the noise and preserving large differences. Bioinformatics 35, 2084–2092. https://doi.org/10.1093/bioinformatics/bty895.